Dalton Transactions

ROYAL SOCIETY OF CHEMISTRY

PAPER

View Article Online
View Journal

Cite this: DOI: 10.1039/d0dt02688c

Reversible switching between housane and cyclopentanediyl isomers: an isonitrile-catalysed thermal reverse reaction†

Henrik Beer, [a] Jonas Bresien, *[a] Dirk Michalik,[a,b] Axel Schulz *[a,b,c] and Alexander Villinger [a]

Received 31st July 2020,
Accepted 24th August 2020

DOI: 10.1039/d0dt02688c

rsc.li/dalton

The photo-isomerization of an isolable five-membered singlet biradical based on C, N, and P ([TerNP]$_2$CNDmp, **2a**) selectively afforded a closed-shell housane-type isomer (**3a**) by forming a transannular P–P bond. In the dark, the housane-type species re-isomerized to the biradical, resulting in a fully reversible overall process. In the present study, the influence of *t*BuNC on the thermal reverse reaction was investigated: the isonitrile acted as a catalyst, thus allowing control over the thermal reaction rate. Moreover, *t*BuNC also reacted with the biradical to form an adduct species ([TerNP]$_2$CNDmp·CN*t*Bu, **4a**), which can be regarded as the resting state of the system. The reactive species **2a** and **3a** could be re-generated *in situ* by irradiation with red light. The results of this study extend our understanding of this new class of molecular switches.

Introduction

Singlet biradicals (also known as biradicaloids) are worthwhile target molecules in synthetic chemistry.[1–5] Due to their unique electronic structure,[6–10] they combine high reactivity with interesting properties such as small molecule activation,[11–14] non-linear optical properties,[15,16] or (potential) applicability as molecular switches.[16–23] Especially for the latter use, it is desirable to devise systems whose two (meta-)stable states possess different degrees of biradical character, so the biradical character[6,8,24–26] can be influenced by an outside stimulus.[27–30]

As stable photo-switchable biradicals are barely known,[22,31–33] we recently started to investigate the photochemistry of five-membered heterocycles, namely hetero-cyclopentanediyls (**2**) generated from the four-membered biradical [P(μ-NR)]$_2$ (**1**, Scheme 1).[20,21] In two recent publications[23,34] we could show that these five-membered biradicals can be reversibly switched to the corresponding housane-type isomer (**3**) using red light, while the reverse reaction takes place under thermal regime.

The reversibility of the process and stability of the isomers **2** and **3** are noteworthy considering that analogous carbon-based cyclopentane-1,3-diyls are usually short-lived and their isomerization to housane or cyclopentene derivatives is typically irreversible,[4,35–38] with few exemptions.[32,33] Also, the photoisomerization of a related heterocyclic housane was found to be irreversible.[39]

Since the housane-type species **3** does not possess significant biradical character, as opposed to the biradical **2** (β = 24–27%),[23,34] switching between these two isomers also allows reversible manipulation of the biradical character. In particular, switching the biradical character "on" and "off" made it possible to influence a (thermal) equilibrium reaction, which involved the activation of *t*BuNC by biradical **2** (Scheme 2).[23]

Interestingly, it was noted that the concentration of *t*BuNC could influence the rate of the thermal reverse reaction **3** → **2**,[23] indicating a catalytic effect of the isonitrile. This prompted us to investigate the mechanism of the thermal reverse reaction in more detail, so as to understand the reactivity of the

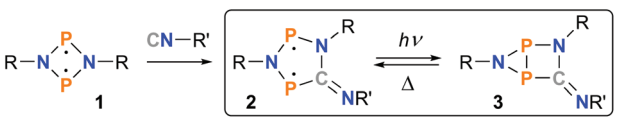

Scheme 1 Synthesis and photochemistry of hetero-cyclopentanediyls (**2**). R = Ter (2,6-dimesitylphenyl), Hyp (tris(trimethylsilyl)silyl); R′ = Mes (mesityl), Dmp (2,6-dimethylphenyl), *t*Bu. Similar compounds can be obtained by reaction of **1** with CO (not shown).

[a]*Institute of Chemistry, University of Rostock, Albert-Einstein-Straße 3a, 18059 Rostock, Germany. E-mail: jonas.bresien@uni-rostock.de, axel.schulz@uni-rostock.de*
[b]*Leibniz Institute for Catalysis, Albert-Einstein-Straße 29a, 18059 Rostock, Germany*
[c]*Department Life, Light & Matter, University of Rostock, 18051 Rostock, Germany*

†Electronic supplementary information (ESI) available: Syntheses, equipment, analytical data, reaction kinetics, computations. CCDC 2013704. For ESI and crystallographic data in CIF or other electronic format see DOI: 10.1039/d0dt02688c

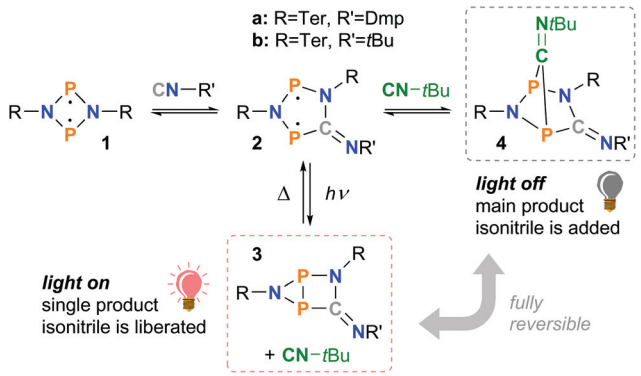

Scheme 2 The molecular switch **2** could be utilized to control a chemical equilibrium reaction involving the activation of *t*BuNC by **2**. The equilibrium with **1** is only observed for **2b**.

housane **3** towards *t*BuNC in comparison with the activation chemistry of biradical **2**. Being the most stable derivative,[21,23,34] the Ter and Dmp substituted variant of **2** (*i.e.* **2a**, R = Ter, R′ = Dmp) was chosen for these investigations.

Results and discussion

Molecular structure

As previously observed in NMR experiments,[23] the reaction of **2a** with *t*BuNC led to formation of adduct **4a** (Scheme 3). As it had only been characterized spectroscopically, it was of interest to isolate and fully characterize adduct **4a**. This could be accomplished by using the isonitrile as solvent (*i.e.* in a large excess) and slowly evaporating the isonitrile until colourless crystals of the desired product **4a** were obtained.

Compound **4a** crystallized in the monoclinic space group *C*2/*c* with 8 formula units per cell. As expected, the five-membered N_2P_2C ring system of the former biradical moiety adopts an envelope conformation, contrary to the planar structure of the free biradical **2a** (Fig. 1).[23] The two P atoms are bridged by the C atom of the former isonitrile moiety, resulting in a [2.1.1]-bicyclic structure; that is, the adduct can be regarded as a [2 + 1] cycloaddition product of the biradical **2a** and *t*BuNC. It is worthy to note that the P1/P2–C58 bond lengths (1.888(1), 1.937(1) Å) are somewhat longer than typical P–C single bonds ($\sum r_{cov}$ = 1.86 Å),[40] indicating a rather weak interaction. This is in agreement with the fact that the adduct formation is a reversible equilibrium reaction (*vide infra*). The overall structure is similar to other derivatives of **4a** with different substituents.[21]

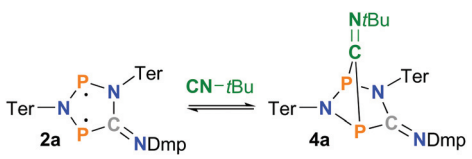

Scheme 3 *t*BuNC could be activated using biradical **2a**, leading to formation of adduct **4a**.

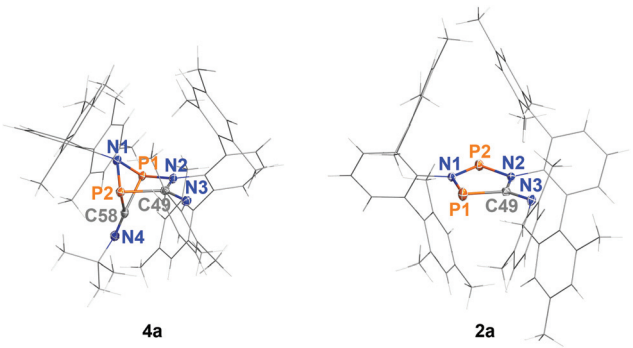

Fig. 1 Left: molecular structure of the adduct **4a** in the crystal. Right: the molecular structure of the biradical **2a** is depicted for comparison.[23] Thermal ellipsoids set at 50% probability (123 K). Selected bond lengths (Å) and angles (°): **4a**: P1–N1 1.779(1), P1–N2 1.734(1), P1–C58 1.888(1), P2–N1 1.776(1), P2–C49 1.880(1), P2–C58 1.937(1), N2–C49 1.403(2), N3–C49 1.270(2), N4–C58 1.250(2), N1–P2–P1–N2 116.57(7); **2a**: P1–N1 1.729(1), P1–C49 1.792(2), P2–N1 1.649(1), P2–N2 1.680(1), N2–C49 1.430(2), N3–C49 1.287(2), N1–P1–P2–N2 178.5(1).

Photoisomerization and thermal reverse reaction

When dissolving colourless crystals of adduct **4a** in THF or benzene, a blue solution was obtained. This could be attributed to partial dissociation of the adduct, which led to partial formation of the blue biradical **2a** and *t*BuNC in an equilibrium mixture with adduct **4a** (*cf.* Scheme 3). The mixture was then irradiated with red light (638 nm) in the NMR spectrometer, resulting in partial formation of the photoproduct **3a** (70%, Scheme 4). All these reactions could easily be traced by ^{31}P NMR spectroscopy, owing to the distinct AX spin systems of **2a** (221.7, 258.3 ppm; 136 Hz), **3a** (−129.1, −63.4 ppm; 65 Hz), and **4a** (188.2, 222.7 ppm; 33 Hz). The experimental data correspond well to calculated values (Table S4†).

In contrast to irradiation of the pure biradical **2a** or the equilibrium mixture associated with **2b** (*cf.* Scheme 2),[23] it was

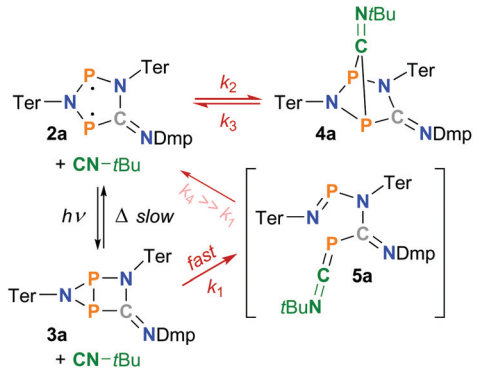

Scheme 4 The thermal reverse reaction **3a** → **2a** was found to be catalysed by *t*BuNC. The reactions considered for the kinetic model are highlighted in red.

however not possible to achieve full photoconversion; species **2a** and **4a** were detectible in the ^{31}P NMR spectrum even under irradiation (20% and 10%, respectively). Moreover, the thermal equilibrium mixture was restored almost instantly when the light source was switched off, indicating a rather fast thermal reverse reaction. (Note that for the *pure* system **2a** ⇄ **3a**, the half-life of **3a** was about 7 minutes at ambient temperature.)[23]

These findings implied that the presence of *t*BuNC had an influence on the rate of the thermal reverse reaction **3a** → **2a**. This could be confirmed by low-temperature NMR experiments using different concentrations of *t*BuNC, which showed a direct proportionality between the rate of the thermal reverse reaction and the *t*BuNC concentration (Scheme 4 and ESI, p. S20ff†). It follows that besides the intramolecular P–P bond cleavage of **3a** (as observed for the pure system **2a** ⇄ **3a**), there must be an alternative pathway for the isomerization of the housane **3a** to the biradical **2a**, involving a reaction between *t*BuNC and **3a**.

Reaction mechanism

To further shed light on the reaction mechanism, the reverse reaction was traced by ^{31}P NMR spectroscopy at different temperatures and at different concentrations of *t*BuNC. The NMR spectra were used to estimate the concentrations of all species in solution, and the time-dependent concentration data were then used to fit a kinetic model involving a second order reaction step between *t*BuNC and **3a** (rate constant k_1, Scheme 4). As the putative intermediate **5a** (or any other intermediates) could not be observed spectroscopically, it was assumed that the reaction step *t*BuNC + **3a** was the rate determining step, *i.e.* all reaction steps between **5a** and **2a** were much faster ($k_4 \gg k_1$) and therefore negligible. Also, taking into consideration that the thermal reverse reaction was orders of magnitude faster in the presence of *t*BuNC, the thermal equilibration of **3a** *via* intramolecular P–P bond cleavage was neglected (Scheme 4).

The above considerations led to the following rate equations

$$\frac{d[\mathbf{2a}]}{dt} = +k_1[\mathbf{3a}][t\text{BuNC}] - k_2[\mathbf{2a}][t\text{BuNC}] + k_3[\mathbf{4a}]$$

$$\frac{d[\mathbf{3a}]}{dt} = -k_1[\mathbf{3a}][t\text{BuNC}]$$

$$\frac{d[\mathbf{4a}]}{dt} = +k_2[\mathbf{2a}][t\text{BuNC}] - k_3[\mathbf{4a}]$$

$$\frac{d[t\text{BuNC}]}{dt} = -k_2[\mathbf{2a}][t\text{BuNC}] + k_3[\mathbf{4a}]$$

where [**2a**], [**3a**], [**4a**], and [*t*BuNC] are the concentrations of **2a**, **3a**, **4a**, and *t*BuNC, respectively, and t is the reaction time. The differential equations were used in a non-linear fitting procedure (ESI, p. S21ff†) to obtain the parameters k_1, k_2, and k_3 as well as the initial concentrations of all species ([**2a**]$_0$, [**3a**]$_0$, [**4a**]$_0$, [*t*BuNC]$_0$) for all different temperatures and concentrations of *t*BuNC (Fig. 2 and ESI, p. S26ff†).

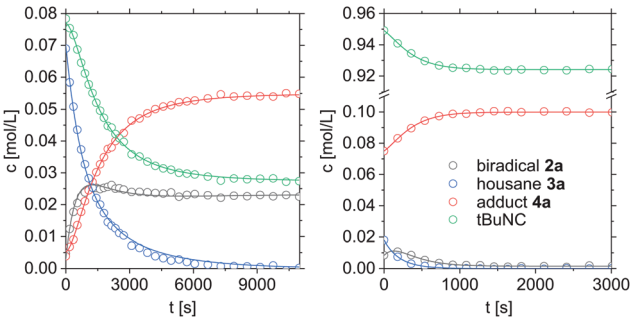

Fig. 2 Thermal reverse reaction **3a** → **2a** in the presence of *t*BuNC. Left: −20 °C, 1 equiv. *t*BuNC. Right: −30 °C, 10 equiv. *t*BuNC. Experimental data plotted as circles; fit functions plotted as solid lines. For more temperatures and concentrations of *t*BuNC, please refer to the ESI, p. S26ff.†

Most importantly, the same rate constants were obtained when the concentration of *t*BuNC was varied and the temperature left unchanged (ESI†), in agreement with the consideration that k_1 is associated with a second order reaction. The temperature dependence of the rate constants was then exploited to estimate the activation barriers of the three reactions associated with k_1, k_2, and k_3 using transition state theory (Table 1, Fig. S11†). This gave $\Delta G^{\ddagger} = 75.9(6)$ kJ mol^{-1} for the reaction of *t*BuNC and **3a** at 298.15 K, which is lower than the activation barrier of intramolecular P–P bond cleavage ($\Delta G^{\ddagger} = 88(4)$ kJ mol^{-1})[23] in accordance with experimental observation.

Moreover, it became evident from the concentration plots in Fig. 2 that the adduct **4a** was the main product of the thermal reverse reaction, *i.e.* it can be regarded as the resting state of the system. Upon irradiation, the equilibrium was perturbed and the thermal reaction was formally shifted back to $t=0$, yielding the housane **3a** and free *t*BuNC as main products. In the dark, the system relaxed to $t \to \infty$. As indicated, this process is fully reversible and can be repeated many times (>20) without detectable degradation of the system.

Computational study

The experimental data clearly demonstrated that the housane **3a** reacted with *t*BuNC in a catalytic manner. However, up to this point, it remained unclear what the nature of the intermediate **5a** was, as it could not be observed in any of the NMR spectra. We therefore decided to perform DFT and *ab initio* cal-

Table 1 Experimental enthalpies and entropies of activation

Step	$\Delta H^{\ddagger}$ [kJ mol^{-1}]	$\Delta S^{\ddagger}$ [J (mol K)$^{-1}$]	$\Delta G^{\ddagger}_{298K}$ [a] [kJ mol^{-1}]
1 (k_1)	42.2 ± 0.3	−113 ± 1	75.9 ± 0.6
2 (k_2)	43 ± 3	−106 ± 11	74 ± 6
3 (k_3)	67 ± 6	−50 ± 23	82 ± 13

[a] Extrapolated values. The rate constants could only be determined at lower temperatures due to the high reaction rates at ambient temperature.

culations to investigate the reactivity of housane **3a** towards *t*BuNC.

In a first step, a model system was chosen to obtain an initial impression of what the reaction between the housane and isonitrile might look like. To this end, all substituents (Ter, Dmp, *t*Bu) were replaced by methyl groups. Using this truncated model (**2c**, **3c**), loose van der Waals complexes of **3c** and MeNC as well as **2c** and MeNC were optimized. These were then used as fixed end points for the calculation of a Nudged Elastic Band (NEB)[41–46] trajectory, which resulted in an approximate Minimum Energy Path (MEP) connecting the two end points on the Potential Energy Surface (PES). Optimization of all stationary points as well as additional Intrinsic Reaction Coordinate (IRC)[47,48] scans resulted in two possible reaction pathways that encompass a nucleophilic attack of the isonitrile at one of the P atoms of the housane as rate determining step (*via* **TS1**), leading to open-chain intermediate **5c** (Fig. 3). Further reaction steps leading to the biradical **2c** and free isonitrile involved either a nucleophilic attack by the N1 atom (*via* **TS2**) or an addition of the N4 atom to the second P atom (**TS4**), followed by [2 + 2] cycloreversion (**TS5**). All these steps exhibited very low activation barriers; thus, it would be expected that the concentration of all possible intermediates would be close to zero throughout the reaction (Fig. 3).

Additionally, the intramolecular P–P bond cleavage was calculated (*via* **TS0**), similarly to what was reported before for the reaction of the pure system **2a** ⇄ **3a**.[23] In comparison with the isonitrile-catalysed reaction, the activation energy ($\Delta G^{\ddagger}$) of the intramolecular pathway is some 17 kJ mol^{-1} higher, in agreement with our experimental observations.

Next, it was of interest to determine if the same reaction pathway could also be found in case of the "real" system **3a** + *t*BuNC → **2a** + *t*BuNC. To keep matters simple and reduce the computational effort, we decided only to investigate the shorter pathway *via* **TS2** (highlighted in red in Fig. 3) and the intramolecular P–P bond cleavage *via* **TS0** (grey). Indeed, the results implied that the same nucleophilic attack of *t*BuNC is possible in case of **3a** despite the presence of the bulky substituents, and that it has a lower activation barrier than the intramolecular P–P bond cleavage (Fig. 4). The calculated energies of **TS0** and **TS1** are somewhat larger than the experimental activation energies, but this is likely attributed to some multireference character of the species involved, which is expected to decrease the accuracy of these calculations (*cf.* ESI p. S29f†). Moreover, we did not include any solvent effects in our calculations. Nonetheless, the experimental trends are well reflected in the computational model. In particular, the computed mechanism also predicts the addition of *t*BuNC to housane **3a** to be the rate determining step, in agreement with the kinetic model derived from NMR data.

Taking into consideration that a side-on adduct of the isonitrile and biradical was found in the model system (*cf.* **A3** in Fig. 3), we were also interested in different adduct types of the actual biradical **2a**. Given that the end-on adduct **4a** was identified as the "resting state" of the system, it seemed particularly interesting to see if a side-on adduct might play a role in the reactivity of the biradical **2a** or the housane **3a**.

Contrary to the model system, though, our computations revealed that the side-on adducts (stationary points **A2** and **A3** in Fig. 4) of *t*BuNC and the biradical **2a** are much higher in energy than the end-on adduct **4a**. This agrees with the absence of other adduct species in the NMR spectra, and

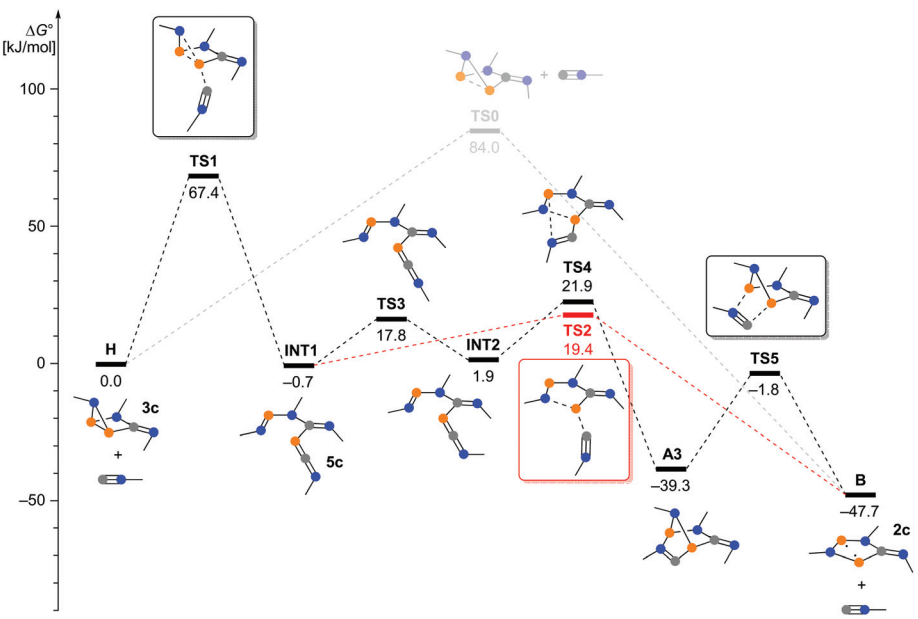

Fig. 3 Thermal reverse reaction of the model housane **3c** (UPBE-D3/def2-TZVP, $p°$ = 1 atm). The addition of MeNC is the rate determining step, leading to formation of metastable adduct **5c** (stationary point **INT1**). The adduct can react to biradical **2c** *via* two pathways, both of which have very low activation barriers. The shortest path is highlighted in red.

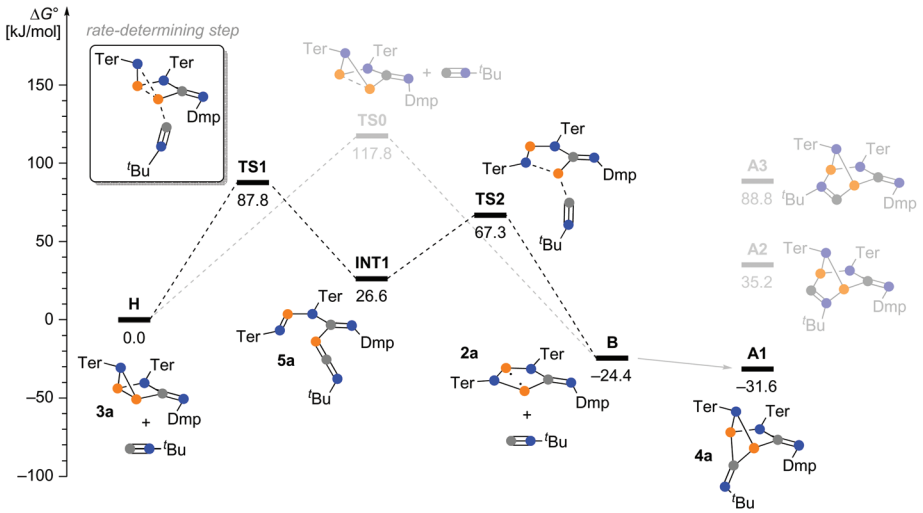

Fig. 4 Computed mechanism for the thermal reverse reaction of the housane **3a** in the presence of *t*BuNC (DLPNO-CCSD(T)/def2-TZVP//UPBE-D3/def2-SVP, $c° = 1$ mol L^{-1}). The reaction with *t*BuNC is energetically favoured in comparison with intramolecular P–P bond cleavage, in agreement with experimental results.

moreover, it indicates that the second reaction pathway found for the model system is most likely not favoured in case of the actual system, due to the large substituents. Furthermore, it is worthy to note that adduct **4a** is predicted to be the global minimum of the reaction coordinate, in accord with experimental observation.

Conclusions

In summary, our investigations of the thermal reverse reaction of the housane **3a** indicate that two distinct isonitrile adducts play an important role for the reactivity of the molecular switch **2a** ⇄ **3a**: firstly, the biradical **2a** can activate the isonitrile in a [2 + 1] cycloaddition reaction, resulting in a [2.1.1]bicyclic structure, which also represents the global minimum of the reaction coordinate. Secondly, the housane **3a** can be activated by the isonitrile in a nucleophilic attack, leading to an unstable open-chain adduct (**5a**) that quickly fragments into the biradical **2a** and the isonitrile. This opens up a different pathway for the thermal reverse reaction of the housane **3a**, and allows chemical control over the rate of the thermal reverse reaction.

Moreover, knowledge of the adduct formation between housane **3a** and isonitrile will help us devise new reactions that take advantage of the nucleophilic activation of the housane. *Inter alia*, this could lead to stable adducts that facilitate trapping of the thermally labile housane species, or even open new avenues in photoswitchable reactions.

Experimental

General information

For detailed information on syntheses, equipment, analytical data, computational methods *etc*. please also consult the ESI.†

All manipulations were carried out under oxygen- and moisture-free conditions under an inert atmosphere of argon using standard Schlenk or Glovebox techniques. NMR spectra under irradiation were recorded using our previously published setup,[23] which was adopted from a setup published by the Gschwind group.[49]

Syntheses

Biradical **2a** was synthesized according to a modified literature procedure.[23] To a solution of $[P(\mu\text{-NTer})]_2$ (459 mg, 0.640 mmol) in benzene (10 mL), DmpNC (82 mg, 0.64 mmol) was added. An immediate colour change from red to deep blue was observed. After two hours the solvent was removed, and the blue residue was dried *in vacuo* (1×10^{-3} mbar). The product was crystallized from a minimal amount of fresh benzene at ambient temperature. The supernatant was removed by syringe and the crystals were dried *in vacuo* (1×10^{-3} mbar). Yield: 480 mg (0.560 mmol, 88%). Mp. 207 °C. CHN calcd (found) in %: C 80.73 (80.36), H 7.01 (6.54), N 4.95 (4.81). $^{31}P\{^1H\}$ NMR (C_6D_6, 202.5 MHz): δ = 221.7 (d, $^2J(^{31}P, ^{31}P)$ = 136 Hz, 1P, N*P*C), 258.3 (d, $^2J(^{31}P, ^{31}P)$ = 136 Hz, 1P, N*P*N). A full set of analytical data can be found in the ESI.†

Adduct **4a**: biradical **2a** (60 mg, 0.07 mmol) was dissolved in *t*BuNC (1.849 mg, 2.5 mL, 22.1 mmol). The light blue solution was stored at −20 °C. Only a few colorless crystals could be collected. Yield <20%. Mp. 148 °C. CHN calcd (found) in %: C 79.97 (79.05), H 7.36 (7.18), N 6.02 (5.87). Deviations due to adhering impurities, *cf*. ESI.† $^{31}P\{^1H\}$ NMR (243 K, THF-d_8, 101.5 MHz): δ = 188.2 (d, $^2J(^{31}P,^{31}P)$ = 33 Hz, 1P, N*P*C), 222.7 (d, $^2J(^{31}P,^{31}P)$ = 33 Hz, 1P, N*P*N). Additional analytical data can be found in the ESI.†

Kinetic studies

To investigate the thermal reverse reaction **3a** → **2a** in the presence of *t*BuNC, solutions of the biradical **2a** with different con-

centrations of *t*BuNC were irradiated in the NMR spectrometer (optical power output approx. 200 mW). When a dynamic steady-state between photoconversion (**2a** → **3a**) and thermal reverse reaction (**3a** → **2a**) was reached, the laser diode was turned off and the thermal equilibration (Fig. S5†) was traced by *in situ* ^{31}P NMR spectroscopy. The concentrations of all species were inferred from the time-resolved NMR spectra. Using a non-linear fitting procedure, the differential rate equations were fitted to the experimental data, yielding the rate constants as fitting parameters. For more details, please refer to the ESI, p. S20ff.†

Computational methods

Computations were carried out using ORCA 4.2.1[46] and Gaussian 09.[50] Structure optimizations were performed using the PBE exchange–correlation functional[51,52] in conjunction with Grimme's dispersion correction D3(BJ)[53,54] and Ahlrichs's def2 basis set family.[55] Accurate electronic energies for optimized structures were computed by single-point DLPNO-CCSD(T)[56–59] calculations employing the def2-TZVP basis set[55] and def2-TZVP/C correlation fitting basis.[60]

Transition states were located on the PES using the Nudged Elastic Band (NEB) algorithm[41–45] implemented in ORCA at the PBE-D3/def2-TZVP level of theory. All transition state (TS) structures were verified to be connected to the corresponding minima using Intrinsic Reaction Coordinate (IRC)[47,48] scans.

For further details (including optimized structures, electronic and thermal energies, NMR data) please refer to the ESI, p. S29ff.†

Conflicts of interest

There are no conflicts to declare.

Acknowledgements

We thank the University of Rostock for access to the high-performance computing facilities, and especially Malte Willert for his assistance with the queueing system and software installations. Special thanks are due to Peter Kumm and Thomas Kröger-Badge for their continuous commitment in our institute's technical and electrical workshops. Furthermore, we wish to thank the DFG (SCHU/1170/12-2) for financial support.

Notes and references

1 H. Grützmacher and F. Breher, *Angew. Chem., Int. Ed.*, 2002, **41**, 4006–4011.
2 F. Breher, *Coord. Chem. Rev.*, 2007, **251**, 1007–1043.
3 M. Abe, J. Ye and M. Mishima, *Chem. Soc. Rev.*, 2012, **41**, 3808–3820.
4 M. Abe, *Chem. Rev.*, 2013, **113**, 7011–7088.
5 S. González-Gallardo and F. Breher, in *Comprehensive Inorganic Chemistry II*, Elsevier, 2013, vol. 1, pp. 413–455.
6 L. Salem and C. Rowland, *Angew. Chem., Int. Ed. Engl.*, 1972, **11**, 92–111.
7 *Diradicals*, ed. W. T. Borden, Wiley-Interscience, New York, 1982.
8 E. Miliordos, K. Ruedenberg and S. S. Xantheas, *Angew. Chem., Int. Ed.*, 2013, **52**, 5736–5739.
9 G. Gryn'ova, M. L. Coote and C. Corminboeuf, *Wiley Interdiscip. Rev.: Comput. Mol. Sci.*, 2015, **5**, 440–459.
10 T. Stuyver, B. Chen, T. Zeng, P. Geerlings, F. De Proft and R. Hoffmann, *Chem. Rev.*, 2019, **119**, 11291–11351.
11 A. Hinz, R. Kuzora, U. Rosenthal, A. Schulz and A. Villinger, *Chem. – Eur. J.*, 2014, **20**, 14659–14673.
12 A. Hinz, R. Kuzora, A.-K. Rölke, A. Schulz, A. Villinger and R. Wustrack, *Eur. J. Inorg. Chem.*, 2016, **2016**, 3611–3619.
13 J. Bresien, A. Hinz, A. Schulz and A. Villinger, *Dalton Trans.*, 2018, **47**, 4433–4436.
14 J. Bresien, A. Hinz, A. Schulz and A. Villinger, *Eur. J. Inorg. Chem.*, 2018, **2018**, 1679–1682.
15 J.-J. Wang, Z.-J. Zhou, H.-M. He, D. Wu, Y. Li, Z.-R. Li and H.-X. Zhang, *J. Phys. Chem. C*, 2016, **120**, 13656–13666.
16 K. Okuno, Y. Shigeta, R. Kishi and M. Nakano, *J. Phys. Chem. Lett.*, 2013, **4**, 2418–2422.
17 H. Li, A. C. Fahrenbach, A. Coskun, Z. Zhu, G. Barin, Y.-L. Zhao, Y. Y. Botros, J.-P. Sauvage and J. F. Stoddart, *Angew. Chem., Int. Ed.*, 2011, **50**, 6782–6788.
18 A. T. Buck, J. T. Paletta, S. A. Khindurangala, C. L. Beck and A. H. Winter, *J. Am. Chem. Soc.*, 2013, **135**, 10594–10597.
19 J. Sun, Y. Wu, Y. Wang, Z. Liu, C. Cheng, K. J. Hartlieb, M. R. Wasielewski and J. F. Stoddart, *J. Am. Chem. Soc.*, 2015, **137**, 13484–13487.
20 A. Hinz, A. Schulz and A. Villinger, *Angew. Chem., Int. Ed.*, 2015, **54**, 2776–2779.
21 A. Hinz, A. Schulz and A. Villinger, *J. Am. Chem. Soc.*, 2015, **137**, 9953–9962.
22 P. Ravat, T. Šolomek, D. Häussinger, O. Blacque and M. Juríček, *J. Am. Chem. Soc.*, 2018, **140**, 10839–10847.
23 J. Bresien, T. Kröger-Badge, S. Lochbrunner, D. Michalik, H. Müller, A. Schulz and E. Zander, *Chem. Sci.*, 2019, **10**, 3486–3493.
24 K. Yamaguchi, *Chem. Phys. Lett.*, 1975, **33**, 330–335.
25 V. Bachler, G. Olbrich, F. Neese and K. Wieghardt, *Inorg. Chem.*, 2002, **41**, 4179–4193.
26 D. Herebian, K. E. Wieghardt and F. Neese, *J. Am. Chem. Soc.*, 2003, **125**, 10997–11005.
27 M.-M. Russew and S. Hecht, *Adv. Mater.*, 2010, **22**, 3348–3360.
28 J. L. Zhang, J. Q. Zhong, J. D. Lin, W. P. Hu, K. Wu, G. Q. Xu, A. T. S. Wee and W. Chen, *Chem. Soc. Rev.*, 2015, **44**, 2998–3022.
29 D. Bléger and S. Hecht, *Angew. Chem., Int. Ed.*, 2015, **54**, 11338–11349.
30 P. C. Knipe, S. Thompson and A. D. Hamilton, *Chem. Sci.*, 2015, **6**, 1630–1639.
31 E. Niecke, A. Fuchs and M. Nieger, *Angew. Chem., Int. Ed.*, 1999, **38**, 3028–3031.

32 M. Abe, E. Kubo, K. Nozaki, T. Matsuo and T. Hayashi, *Angew. Chem., Int. Ed.*, 2006, **45**, 7828–7831.
33 S. Yoshidomi and M. Abe, *J. Am. Chem. Soc.*, 2019, **141**, 3920–3933.
34 H. Beer, J. Bresien, D. Michalik, A.-K. Rölke, A. Schulz, A. Villinger and R. Wustrack, *J. Org. Chem.*, 2020, acs.joc.0c00460.
35 W. Adam, W. T. Borden, C. Burda, H. Foster, T. Heidenfelder, M. Heubes, D. A. Hrovat, F. Kita, S. B. Lewis, D. Scheutzow and J. Wirz, *J. Am. Chem. Soc.*, 1998, **120**, 593–594.
36 F. Kita, W. Adam, P. Jordan, W. M. Nau and J. Wirz, *J. Am. Chem. Soc.*, 1999, **121**, 9265–9275.
37 D. Y. Zhang, D. A. Hrovat, M. Abe and W. T. Borden, *J. Am. Chem. Soc.*, 2003, **125**, 12823–12828.
38 M. Abe, W. Adam, W. T. Borden, M. Hattori, D. A. Hrovat, M. Nojima, K. Nozaki and J. Wirz, *J. Am. Chem. Soc.*, 2004, **126**, 574–582.
39 B. J. Guddorf, C. Mück-Lichtenfeld, A. Hepp and F. Lips, *Chem. Commun.*, 2019, **55**, 12896–12899.
40 P. Pyykkö and M. Atsumi, *Chem. – Eur. J.*, 2009, **15**, 12770–12779.
41 G. Mills, H. Jónsson and G. K. Schenter, *Surf. Sci.*, 1995, **324**, 305–337.
42 H. Jónsson, G. Mills and K. W. Jacobsen, in *Classical and Quantum Dynamics in Condensed Phase Simulations*, World Scientific, 1998, pp. 385–404.
43 G. Henkelman and H. Jónsson, *J. Chem. Phys.*, 2000, **113**, 9978–9985.
44 G. Henkelman, B. P. Uberuaga and H. Jónsson, *J. Chem. Phys.*, 2000, **113**, 9901–9904.
45 E. Maras, O. Trushin, A. Stukowski, T. Ala-Nissila and H. Jónsson, *Comput. Phys. Commun.*, 2016, **205**, 13–21.
46 F. Neese, *Wiley Interdiscip. Rev.: Comput. Mol. Sci.*, 2018, **8**, e1327.
47 K. Ishida, K. Morokuma and A. Komornicki, *J. Chem. Phys.*, 1977, **66**, 2153–2156.
48 K. Fukui, *Acc. Chem. Res.*, 1981, **14**, 363–368.
49 C. Feldmeier, H. Bartling, E. Riedle and R. M. Gschwind, *J. Magn. Reson.*, 2013, **232**, 39–44.
50 M. J. Frisch, G. W. Trucks, H. B. Schlegel, G. E. Scuseria, M. A. Robb, J. R. Cheeseman, G. Scalmani, V. Barone, B. Mennucci, G. A. Peterson, H. Nakatsuji, M. Caricato, X. Li, H. P. Hratchian, A. F. Izmaylov, J. Bloino, G. Zheng, J. L. Sonnenberg, M. Hada, M. Ehara, K. Toyota, R. Fukuda, J. Hasegawa, M. Ishida, T. Nakajima, Y. Honda, O. Kitao, H. Nakai, T. Vreven, J. A. Montgomery Jr., J. E. Peralta, F. Ogliaro, M. Bearpark, J. J. Heyd, E. Brothers, K. N. Kudin, V. N. Staroverov, T. Keith, R. Kobayashi, J. Normand, K. Raghavachari, A. Rendell, J. C. Burant, S. S. Iyengar, J. Tomasi, M. Cossi, N. Rega, J. M. Millam, M. Klene, J. E. Know, J. B. Cross, V. Bakken, C. Adamo, J. Jaramillo, R. Gomperts, R. E. Stratmann, O. Yazyev, A. J. Austin, R. Cammi, C. Pomelli, J. W. Ochterski, R. L. Martin, K. Morokuma, V. G. Zakrezewski, G. A. Voth, P. Salvador, J. J. Dannenberg, S. Dapprich, A. D. Daniels, O. Farkas, J. B. Foresman, J. V. Ortiz, J. Cioslowski and D. J. Fox, *Gaussian 09, Revision E.01*, Gaussian, Inc., Wallingford CT, 2013.
51 J. P. Perdew, K. Burke and M. Ernzerhof, *Phys. Rev. Lett.*, 1996, **77**, 3865–3868.
52 J. P. Perdew, K. Burke and M. Ernzerhof, *Phys. Rev. Lett.*, 1997, **78**, 1396–1396.
53 S. Grimme, J. Antony, S. Ehrlich and H. Krieg, *J. Chem. Phys.*, 2010, **132**, 154104.
54 S. Grimme, S. Ehrlich and L. Goerigk, *J. Comput. Chem.*, 2011, **32**, 1456–1465.
55 F. Weigend and R. Ahlrichs, *Phys. Chem. Chem. Phys.*, 2005, **7**, 3297–3305.
56 C. Riplinger and F. Neese, *J. Chem. Phys.*, 2013, **138**, 034106.
57 D. G. Liakos, M. Sparta, M. K. Kesharwani, J. M. L. Martin and F. Neese, *J. Chem. Theory Comput.*, 2015, **11**, 1525–1539.
58 C. Riplinger, P. Pinski, U. Becker, E. F. Valeev and F. Neese, *J. Chem. Phys.*, 2016, **144**, 024109.
59 D. G. Liakos, Y. Guo and F. Neese, *J. Phys. Chem. A*, 2020, **124**, 90–100.
60 A. Hellweg, C. Hättig, S. Höfener and W. Klopper, *Theor. Chem. Acc.*, 2007, **117**, 587–597.